SAND2016-11101J

Shock compression experiments on Lithium Deuteride (LiD) single crystals

M.D. Knudson,[1, 2, a] M.P. Desjarlais,[1] and R.W. Lemke[1]

[1] *Sandia National Laboratories, Albuquerque, NM 87123*

[2] *Institute for Shock Physics, Washington State University, Pullman, WA 99164-2816*

Shock compression experiments in the few hundred GPa (multi-Mbar) regime were performed on Lithium Deuteride (LiD) single crystals. This study utilized the high velocity flyer plate capability of the Sandia Z Machine to perform impact experiments at flyer plate velocities in the range of 17-32 km/s. Measurements included pressure, density, and temperature between ∼190-570 GPa along the Principal Hugoniot – the locus of end states achievable through compression by large amplitude shock waves – as well as pressure and density of reshock states up to ∼920 GPa. The experimental measurements are compared with density functional theory calculations, a tabular equation of state recently developed at Los Alamos National Labs, and legacy nuclear driven results that have been reanalyzed using modern equations of state for the shock wave standards used in the experiments.

---

[a] Electronic mail: mdknuds@sandia.gov

I. INTRODUCTION

Lithium hydride and lithium deuteride (LiH, LiD) represent the simplest alkali hydride and a protoypical ionic solid. As such it has been the focus of many studies, both experimental[1–5]and theoretical.[6–10] LiH is also one of the simplest compounds, making it a model system for studying mixture rules in the warm dense matter regime. Recent quantum molecular dynamics (QMD) and orbital-free molecular dynamics (OFMD) studies have evaluated the use of density and pressure mixing rules for obtaining equation of state (EOS), optical properties, such as frequency dependent absorption coefficients and Rosseland mean opacities, and dynamical properties, such as diffusion and viscosity, over a density and temperature range of 0.5-4 times ambient density and 0.5-6 eV, respectively.[11,12]

However, as illustrated in Fig. 1, comparison of existing EOS models for ^{6}LiD show a significant discrepancy along the Principal Hugoniot – the locus of end states achievable through compression by large amplitude shock waves – in the several hundred GPa (several Mbar) range. In particular, the legacy EOS models at Lawrence Livermore National Labs (LLNL) and Los Alamos National Labs (LANL), X2040[13] and SESAME 7247,[14] respectively, as well as the more modern SESAME 7360[10] and 7363[15] recently developed at LANL, show significant differences even at a few Mbar. Several Mbar dynamic pressure in LiD is readily accessible by high-velocity, plate impact experiments at the Sandia Z Machine.[16] Furthermore, the achievable precision and accuracy for Hugoniot measurements in this regime is sufficient to distinguish between the various EOS models.

Here we present the results of *ab-initio* molecular dynamic (AIMD) calculations and magnetically accelerated flyer plate experiments on single crystal LiD. These data, in the range of 190-570 GPa along the Principal Hugoniot fill a sizable gap between lower pressure (P) gas gun experiments[1] ($P < 80$ GPa) and higher P nuclear driven experiments[2,3] ($P \approx$ 1000 GPa). Temperature for some of these experiments were obtained through the use of radiometry. Furthermore, the present work obtained reshock data for LiD in the range of 730-920 GPa, providing additional constraints for first-principles models in the warm dense matter regime.

These experiments were complicated due to the fact that LiD readily reacts with moisture to form lithium hydroxide (LiOH). This necessitated encapsulation of the samples. We chose to use single crystal α-quartz as a material for encapsulation given that (i) α-quartz

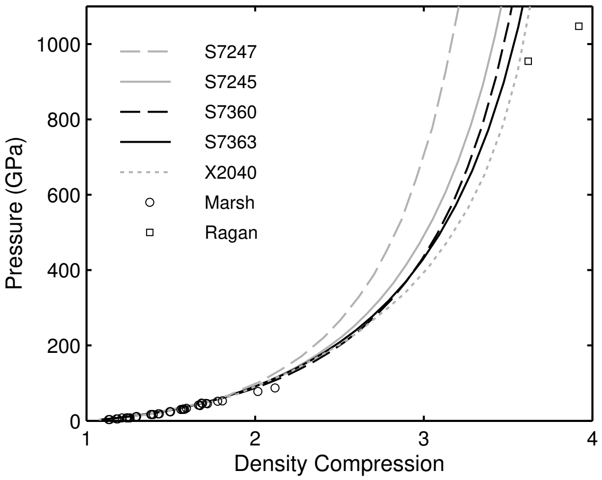

FIG. 1. LiD P-density compression Hugoniot with $\rho_0 = 0.8\ g/cm^3$. *Models*: dashed gray line, SESAME 7247[14]; solid gray line, SESAME 7245[14]; dashed black line, SESAME 7360[10]; solid black line, SESAME 7363[15]; dotted gray line, X2040[13]. *Data*: open circles, Marsh et al.[1]; open squares, Ragan.[2,3]

is transparent, allowing optical access to the LiD sample, and (*ii*) recent Hugoniot[17] and adiabatic release measurements in α-quartz[18] have enabled the use of α-quartz as a high-precision standard for impedance matching measurements in the multi-Mbar regime. This use of α-quartz resulted in a negligible increase in uncertainty in the inferred shock response as compared to the precision achievable through direct impact experiments with aluminum flyer plates.

The experiments are discussed in Sections II and III, including characterization of the single crystal LiD samples and the experimental configuration. The results of the experiments are presented in Section IV, including the density, pressure, and temperature along the Hugoniot, as well as the density and pressure for reshock states. A reanalysis of legacy nuclear driven experiments is presented in Section V and discussed in the context of the present work. The results are summarized in Section VI.

II. SAMPLE CHARACTERIZATION

Single crystal Lithium Deuteride (LiD) sample material was obtained from the Crystal Growth Lab at the University of Utah. The crystal was received in boule form and was cleaved within an argon atmosphere to nominally 4 mm in lateral dimensions and ~0.5-0.8

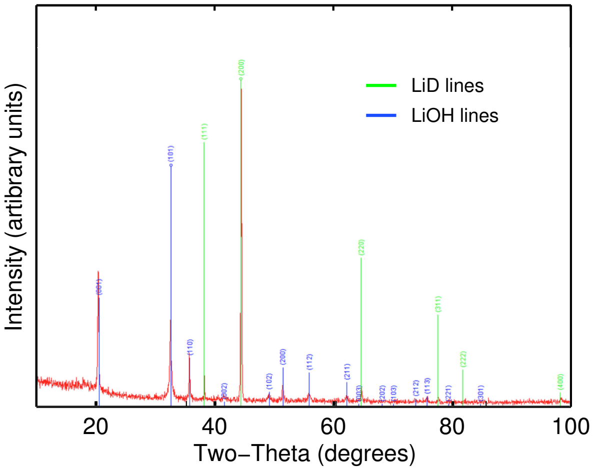

FIG. 2. X-ray diffraction data from a powdered LiD sample between 10-100 degrees in two-theta. Diffraction lines from both crystalline LiD (green lines) and LiOH (blue lines) are observed. The measured LiD lattice parameter was $a = 4.072 \pm 0.003$ Å, resulting in a unit cell volume of 67.52 ± 0.15 Å^3.

mm in thickness prior to encapsulation within an aluminum and α-quartz sample holder. Shards from the cleaving process were used for further sample analysis described below.

A. X-ray Diffraction Measurements

Small LiD shards were ground within a ball mill to prepare a powdered sample. An x-ray diffraction (XRD) pattern was obtained from the powdered sample between 10-100 degrees in two-theta, shown in Fig. 2. Diffraction lines were observed from both LiD and LiOH. The source of the LiOH diffraction lines was likely an opaque layer on the outside of the boule (which was present on some of the shards), presumably a hydroxide layer resulting from reaction of the LiD crystal with either moisture from air prior to the boule being placed in mineral oil for storage, or from moisture within the mineral oil itself. Note that the presence of the hydroxide does not affect the lattice parameter measurement for the LiD crystal, and is thus ignored. The measured lattice parameter was $a = 4.072 \pm 0.003$ Å, resulting in a unit cell volume of 67.52 ± 0.15 Å^3. Given that there are four LiD pairs per unit cell, the molar volume was determined to be 10.165 ± 0.022 cm^3/mol. This allows the density of the sample to be determined given the isotopic fraction of ^{6}Li to ^{7}Li in the sample.

B. Inductively Coupled Plasma Mass Spectrometry Measurements

Small LiD shards were dissolved and used as the sample for inductively coupled plasma mass spectroscopy (ICP-MS) measurements to determine the isotopic concentration of Li in the actual sample material. The results of the measurement indicated a ^{6}Li composition of between 2.2-2.4% and a ^{7}Li composition of between 97.6-97.8%. This is outside of the natural abundance ratio for Li, which has a ^{6}Li and ^{7}Li composition of $7.59 \pm 0.04\%$ and $92.41 \pm 0.04\%$, respectively.[19] These results suggest that the sample material for this study is somewhat ^{7}Li rich, but not pure ^{7}Li.

It was not possible to determine the isotopic ratio of hydrogen to deuterium through ICP-MS. However, the lattice parameter measurement strongly suggests that the sample material for this study was highly deuterium enriched. Fig. 3 shows the measured lattice parameters for ^{6}LiH, ^{n}LiH, ^{7}LiH, ^{6}LiD, ^{n}LiD, and ^{7}LiD, as a function of the molar mass[20] (^{n}Li refers to an isotopic ratio consistent with the natural abundance referred to above). Also shown in Fig. 3 is the measured lattice parameter and the molar mass one would infer for a pure D concentration (black diamond). Given the significantly larger lattice parameter for pure H concentration (black squares) versus the pure D concentration (gray squares), clearly the measured lattice parameter for this sample is consistent with the D isotope. Given the measured Li isotopic concentration, assumed pure D concentration, and the measured molar volume of the crystal sample, one can determine the density of the sample fairly precisely. The density was determined to be 0.886 ± 0.002 g/cm^3, an uncertainty of roughly 0.22%.

C. Refractive Index

The refractive index is important for proper interpretation of the shock velocity in the LiD sample obtained from velocimetry measurements (Section III). Given the fact that LiD readily reacts with moisture and must be handled within an inert environment, an accurate measurement of the refractive index of this particular sample material was not possible. It was determined that the most accurate reported value for the refractive index in the literature was from Ref. 21. That study reported measurement of the refractive index at wavelengths of 435.8, 546.1, and 589.2 nm. Interpolation of these measurements to the wavelength used in this study (532 nm) results in an inferred refractive index of

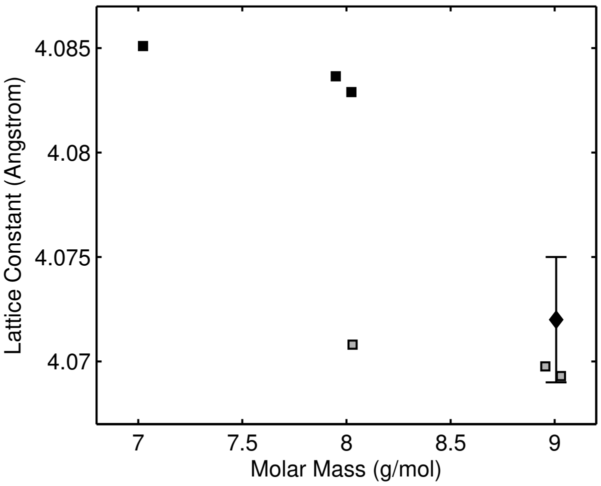

FIG. 3. Measured lattice parameters[20] as a function of molar mass for ^{6}LiH, ^{n}LiH, and ^{7}LiH (black squares), and ^{6}LiD, ^{n}LiD, and ^{7}LiD (gray squares). The measured lattice parameter for the material used in this study was $a = 4.072 \pm 0.003$ Å (black diamond), which is consistent with ^{7}LiD and not consistent with ^{7}LiH.

$n = 2.007 \pm 0.005$. This is the value used in the analysis described in Section III.

III. EXPERIMENTAL CONFIGURATION

A series of planar, plate-impact, shock-wave experiments were performed at the Sandia Z machine,[16] a pulsed power accelerator capable of generating ∼20 MA currents and ∼10 MGauss magnetic fields in a short circuit load. The load, which is nominally 4-5 cm in each dimension, is designed to compress the cathode and explode the anode outward as a flyer-plate,[22,23] producing impact velocities in excess of 30 km/s.

Two different load geometries were used in this study. The first, referred to as a coaxial load, has anode plates completely surrounding a central rectangular cathode stalk.[22] Two of these anode plates are designed to be aluminum flyer-plates with initial dimensions of approximately 40 mm in height, 20 mm in width, and 1 mm in thickness. The anode box is intentionally aligned asymmetric about the cathode stalk, with feed gaps of 1 and 1.4 mm on the two flyer-plate sides. This asymmetry allows for different magnetic pressure in the two gaps, resulting in two different peak flyer-plate velocities for each firing of the Z machine, thereby increasing data return.

The second load geometery, referred to as a stripline load, has a single anode plate opposite a similar cathode plate, with a single feed gap.[23] In this case both the anode and cathode are flyer-plates with initial dimensions of approximately 36 mm in height, 10 mm in width, and 1 mm in thickness. The benefit of this design is that a significantly larger current density is achieved with respect to the coaxial load, thereby enabling higher flyer-plate velocities to be achieved. However, in this case both flyer-plates reach essentially the same impact velocity and thus only a single Hugoniot point is obtained for each firing of the Z machine.

Upon discharge of the stored energy within the Marx capacitor banks, a shaped current pulse of ∼300 ns duration and ∼20 MA in magnitude is directed through the experimental load. The large current induces a large magnetic field and the resulting $\vec{J}$ X $\vec{B}$ force propels the flyer-plates outward. With proper load design and temporal shaping of the current pulse, accelerations of a few tens of giga-g are produced that drive the solid aluminum panels across a 3-5 mm vacuum gap, ultimately reaching impact velocities of 17-32 km/s depending upon the load geometry and the peak charge voltage of the accelerator. More details regarding the flyer-plate launch and the state of the flyer-plates at impact can be found in Refs. 22 and 23.

Single crystal LiD samples were cleaved from a boule obtained from the Crystal Growth Lab at the University of Utah. Nominal sample sizes were ∼4 mm in in lateral dimensions and ∼0.5-0.8 mm in thickness. Given that LiD readily reacts with moisture to form LiOH, the samples were encapsulated within aluminum and α-quartz target holders. The holders, the particular details of which evolved over the experimental series, were essentially aluminum sleeves with single crystal α-quartz windows as end caps. The cleaving and encapsulation were performed within an argon glove box to protect the sample integrity. The target holders were then mounted into a panel back at a prescribed flight distance between 3 and 5 mm, depending upon the desired peak impact velocity.

The flyer plates, α-quartz windows, and LiD samples were diagnosed using a velocity interferometer (VISAR, Velocity Interferometer System for Any Reflector[24]). Since the LiD sample is transparent in the visible spectrum, the 532 nm laser light could pass through the target holder and reflect off the flyer plate surface. This allowed an in-line measurement of the flyer velocity from initial motion to impact. Upon impact a several hundred GPa shock was sent through the α-quartz and LiD sample. This shock was of sufficient magnitude that the resulting plasma became a weak metal, providing significant reflectivity in the visible

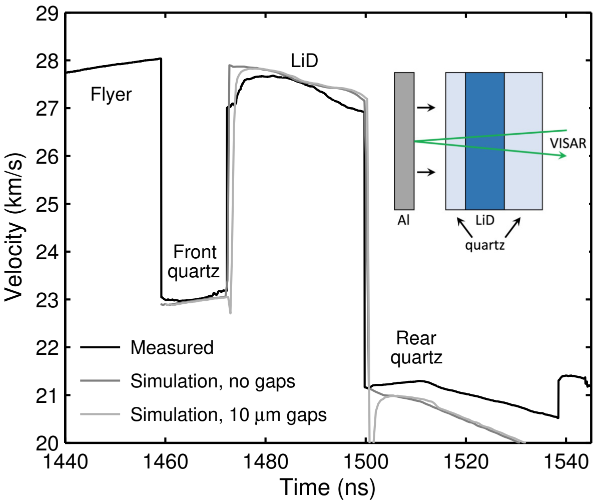

FIG. 4. Representative experimental data: black line, measured velocity profile from VISAR; dark gray line, hydrodynamic simulation with no gaps between the LiD and quartz; light gray line, hydrodynamic simulation with 10 μm gaps between the LiD and quartz.

range. This allowed for direct measurement of the shock velocity of both the α-quartz and LiD with the VISAR diagnostic. Ambiguity in the fringe shift was mitigated through the use of three different VISAR sensitivities or velocity per fringe (vpf) settings.

A correction to the sensitivity of the VISAR diagnostic is necessary to obtain the correct shock velocity in both the α-quartz and LiD sample. This is due to the fact that as the shock transits through an initially transparent material the thickness of the un-shocked material through which the laser passes decreases with time, introducing a further Doppler shift in addition to the Doppler shift produced by the moving shock front. It can be shown that for this case the measured apparent velocity, v_a, must be reduced by a factor equal to the refractive index, n, of the un-shocked material; $v = v_a/n$. The refractive index values used in this study for α-quartz and LiD were 1.547 and 2.007, respectively.[21,25] Representative velocity profiles are shown in Fig. 4.

Note that in the example shown in Fig. 4 the shock velocity in the LiD sample has an initial ramp before saturating at a value of ~27.5 km/s. This was the result of a small gap between the front α-quartz window and the LiD sample. Because the LiD readily reacts with moisture the α-quartz/LiD/α-quartz sample stack was not glued together with epoxy (the typical procedure for these types of experiments). As a result, evidence of small gaps at the front and/or rear interface was observed for most experiments. To determine the effect of these gaps on the analysis of the experiments, several one-dimensional simulations of the experiments were performed using the radiation magneto-hydrodynamic (MHD) code ALEGRA.[26] Typical simulations were pure hydrodynamic simulations started at the moment of impact with a flyer plate initialized with the density, temperature, and velocity profile obtained from a one-dimensional MHD optimization of the flyer plate launch, similar to that described in Ref. 27. The aluminum flyer plate, the front and rear α-quartz windows, and the LiD sample were discretized to 0.5 μm cell sizes and modeled using SESAME equations of state (EOS) 3700,[28] q7360,[29] and 7363,[15] respectively. Note that an isotopically scaled version of SESAME 7363 was used for $^{\mathrm{n}}$LiD.

As can be seen in Fig. 4, the simulations capture qualitatively the behavior observed in the experiment. In particular, the simulated shock velocity in the LiD sample for a simulation that included a 10 μm gap between the front α-quartz window and the LiD sample (light gray line) exhibits a similar ramp in velocity prior to saturation, the result of plasma blow off from the shocked α-quartz front window reverberating between the α-quartz window and the LiD sample. Comparing this simulation with a second simulation that did not include a gap between the front α-quartz window and the LiD sample (dark gray line) suggests that the saturated velocity is a reasonable estimate of the expected shock velocity immediately upon the shock entering the sample.

These small gaps introduced additional complications with the experiment. In particular, the gaps resulted in significant interface reflections, which were especially severe in the first experiment. Given the large refractive index of LiD ($n = 2.007$), dielectric coatings were put on the α-quartz windows to minimize reflections assuming the α-quartz would be directly in contact with the LiD sample. However, with a gap present there are then two interfaces, each with two surfaces of $n = 2$ against $n = 1$ (α-quartz/gap and gap/LiD), resulting in a total reflection of ∼45% (each surface has a reflection of ∼11.1%; see Fig. 8). In an attempt to mitigate these reflections, the subsequent target holders were designed such that a mineral oil based index fluid ($n = 1.7$) could be placed between the α-quartz and LiD sample. This configuration still resulted in reverberation (although the reverberations were mitigated given the relative impedance of the oil to the LiD), however the overall reflections at the interfaces were reduced to a few percent.

Emission from the shocked α-quartz windows and LiD sample were collected in an optical fiber and delivered to a streaked visible spectroscopy (SVS) diagnostic which consisted of a

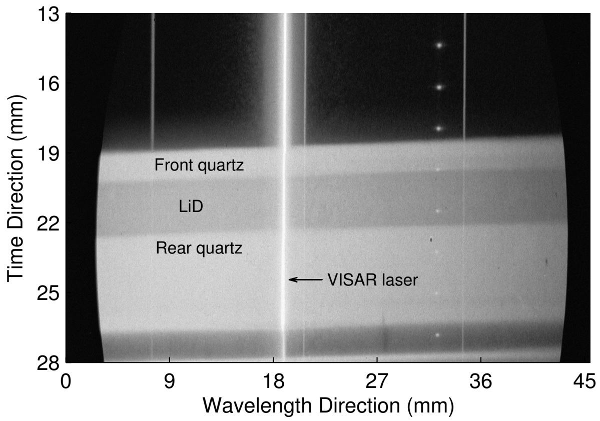

FIG. 5. Representative SVS data showing spectrally and temporally resolved emission; time increases down and wavelength increases to the right.

spectrometer coupled to a streak camera to provide spectrally and temporally resolved data. A typical SVS image is shown in Fig. 5. In this image time is running down and wavelength increases to the right. The first bright horizontal band (around 19-20 mm in the time direction) is emission from the shocked front α-quartz window. The lighter band (between 20-22 mm) is emission from the shocked LiD sample. The next brighter band (between 22-26.5 mm) is emission from the shocked rear α-quartz window. The bright vertical band (near 19 mm in the wavelength direction) corresponds to the 532 nm VISAR laser. The other vertical bands correspond to wavelength (457.9, 543.5, and 632.8 nm) and time (20 ns impulse comb) fiducials. The analysis of these data to infer temperature of the shocked LiD sample will be described in Section IV B.

IV. EXPERIMENTAL RESULTS

A. Principal Hugoniot

The shocked state of the LiD was determined using the impedance matching method and the Rankine-Hugoniot (RH) jump relations.[30] The jump relations, derived by considering conservation of mass, momentum, and energy across a steady propagating shock wave, are a set of equations that relate the initial energy, E, volume, V, and pressure, P, with steady-state, post-shock values:

$$(E_1 - E_0) = (P_1 + P_0)(V_0 - V_1)/2 \tag{1}$$

TABLE I. LiD Hugoniot data. U_s^{Q} and U_s^{LiD} are the measured shock velocities in the front α-quartz window and LiD sample, respectively. u_{p1}, P_1, and ρ_1 are the inferred particle velocity, pressure, and density in the Hugoniot state, respectively.

Expt	U_s^{Q} (km/s)	U_s^{LiD} (km/s)	u_{p1} (km/s)	P_1 (GPa)	ρ_1 (g/cm^3)
Z2586	15.77 ± 0.03	18.92 ± 0.06	11.22 ± 0.07	188.1 ± 1.2	2.178 ± 0.023
Z2497N	23.21 ± 0.03	27.63 ± 0.06	18.65 ± 0.08	456.5 ± 2.1	2.726 ± 0.029
Z2497S	24.75 ± 0.03	29.55 ± 0.06	20.24 ± 0.09	530.0 ± 2.5	2.815 ± 0.031
Z2577	25.21 ± 0.03	30.29 ± 0.06	20.70 ± 0.09	555.6 ± 2.6	2.797 ± 0.030
Z2692	25.46 ± 0.03	30.54 ± 0.06	20.97 ± 0.09	567.5 ± 2.7	2.827 ± 0.031

$$(P_1 - P_0) = \rho_0 U_s \left(u_{p1} - u_{p0}\right) \tag{2}$$

$$\rho_1 = \rho_0 \left[U_s / \left(U_s - \left(u_{p1} - u_{p0}\right)\right)\right] \tag{3}$$

where ρ, U_s, and u_p denote the density, shock velocity, and particle velocity, respectively, and the subscripts 0 and 1 denote initial and final values, respectively.

The shocked state of the α-quartz drive plate was determined by the known α-quartz Hugoniot[17] and the measured α-quartz shock velocity, U_s^{Q}. This defines a point $(P^{\mathrm{Q}}, u_p^{\mathrm{Q}})$ from which the release adiabat emanates. A recently developed α-quartz release model[18] was used to calculate this release path. Given Eq. (2), the shocked state of the LiD is constrained to lie on the Rayleigh line, given by slope $\rho_0 U_s^{\mathrm{LiD}}$. The intersection of the release path and the Rayleigh line provides (P_1, u_{p1}); the remaining kinematic variables are determined through Eqs. (2) and (3). Using a Monte Carlo technique,[31] the one-sigma uncertainties in u_{p1}, P_1, and ρ_1 were found to be ∼0.5%, ∼0.5%, and ∼1%, respectively.

A total of four plate impact experiments, one coaxial and three stripline, were performed on single crystal LiD. The pertinent parameters for these experiments are listed in Table I. U_s^{Q} and U_s^{LiD} denote the measured shock velocities in the front α-quartz window and the LiD sample, respectively. u_{p1} denotes the inferred particle velocity in the LiD, and P_1 and ρ_1 denote the inferred pressure and density of the LiD in the shocked state, respectively. The Hugoniot data for LiD are shown in both $U_s - u_p$ and $P - \rho$ in Figs. 6 and 7.

In addition to the experimental study, we also performed *ab-initio* molecular dynam-

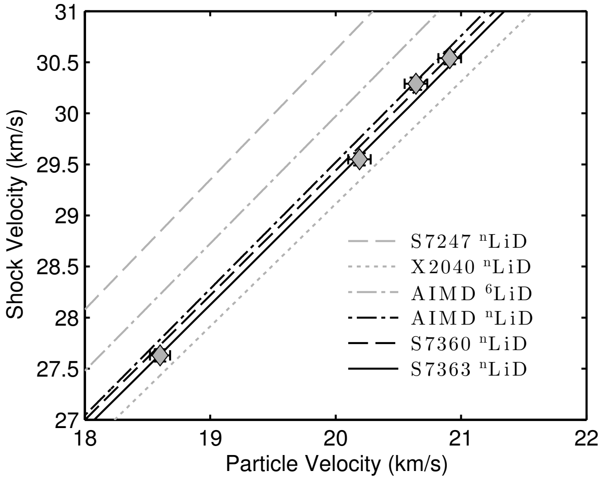

FIG. 6. LiD $U_s - u_p$ Hugoniot. Dot-dashed black (gray) line, AIMD ${}^{\mathrm{n}}$LiD (^{6}LiD), this work. All other lines and symbols as in Fig. 1 for ${}^{\mathrm{n}}$LiD.

ics (AIMD) calculations of the LiD Hugoniot for both ^{6}LiD and ${}^{\mathrm{n}}$LiD. Calculations were performed using the Vienna *ab-initio* simulation program (VASP[32]), a plane-wave density functional theory (DFT) code developed at the Technical University of Vienna. Coulomb interactions between the electrons and ions were treated using projector-augmented wave (PAW) potentials.[33] All calculations performed in this study included 128 atoms in the super cell, plane wave cutoff energies of 1200 eV, and Baldereschi's mean value for the **k**-point. Simulations were done in the canonical ensemble, with simple velocity scaling as a thermostat, and typically covered several picoseconds of real time. Thermodynamic quantities were taken as time averages of the equilibrated portions of the molecular dynamics runs.

The results from the AIMD calculations are shown in Figs. 6 and 7. Also shown are the predicted response from X2040 and SESAME 7247, 7360, and 7363. Note that we only had access to the ^{6}LiD EOS models for both SESAME 7247 and X2040. To account for the higher molar mass of our samples, which are very close to ${}^{\mathrm{n}}$LiD, we performed a simple shift in the $U_s - u_p$ response from these models downward by 0.37 km/s in U_s for a given u_p. This shift was determined by comparison of AIMD calculations for ^{6}LiD and ${}^{\mathrm{n}}$LiD, as well as comparing isotopically scaled versions of the SESAME 7360[10] and 7363[15] EOS models for ^{6}LiD and ${}^{\mathrm{n}}$LiD. The experimental data suggests that the X2040 EOS is systematically too compressible and the SESAME 7247 EOS is significantly too stiff. In contrast, the data are in quite good agreement with the AIMD calculations and the more modern SESAME

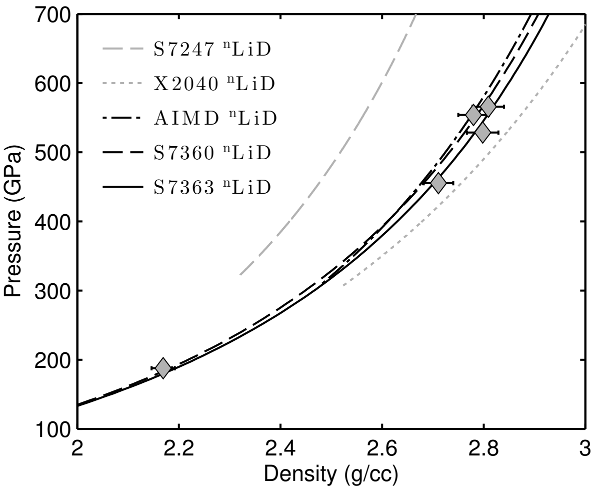

FIG. 7. LiD $P - \rho$ Hugoniot. Lines and symbols as in Fig. 6.

7360[10] and 7363[15] EOS models.

B. Temperature on the Hugoniot

Temperature (T) of the shocked LiD sample was determined by using the emission from the α-quartz front and rear windows as a T standard. Previous shock wave experiments on α-quartz in the multi-Mbar regime have determined the T and reflectivity of α-quartz as a function of shock speed,[34] enabling α-quartz to be used as a standard for T measurements. Emission from the rear α-quartz window was used as a calibration for the SVS image. Given the shock velocity in the rear α-quartz window, and the T and reflectivity of α-quartz at that shock speed, a calibration factor was determined for each SVS image. Furthermore, given the shock velocity in the front α-quartz window, and the T and reflectivity of α-quartz at that shock speed, the emission one would expect to observe from the front α-quartz window was also determined. Typically, the expected emission from the front α-quartz window was greater than what is actually observed; the difference being attributed to reflection loses at the two α-quartz/LiD interfaces (see discussion above). Under the assumption that these two interfaces contribute equally to the reflection losses, the observed LiD emission was corrected accordingly. Finally, given the emissivity of LiD in the multi- Mbar regime, determined through AIMD calculations, the T of the shocked LiD was determined.

This procedure, which is illustrated for a lineout at ∼480 nm in Fig. 8, was followed at

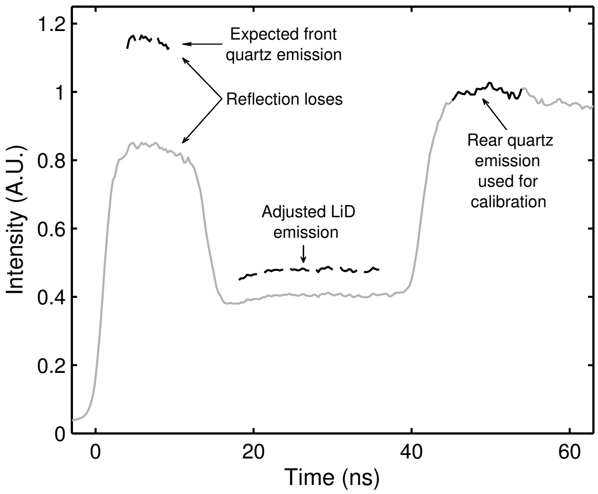

FIG. 8. Relative temperature analysis procedure. The measured U_s^{Q} and emission in the rear quartz window was used to determine a calibration factor for the SVS image at each wavelength. The measured U_s^{Q} in the front window was used to determine the expected emission; the difference between the expected and observed emission provided a measure of reflection loses at each LiD/quartz interface. This was in turn used to adjust the observed emission in the LiD.

each wavelength across the recorded SVS spectrum. A relatively flat inferred T was obtained across the 450-650 nm spectrum, lending confidence in the method used to infer the T of the shocked LiD. The inferred temperature was then averaged across the 450-650 nm spectrum to obtain the LiD T in the shocked state. The inferred T from four of the experiments are shown in Fig. 9. Also shown in Fig. 9 are three AIMD calculations (black circles) and the predictions from SESAME 7360[10] and 7363[15] (dashed and solid black lines, respectively).

C. Reshock

The compressibility of LiD was further explored by performing reshock experiments. In four of the Hugoniot experiments described above, the reflected shock from the rear α-quartz window drove the LiD from a Hugoniot state to a reshocked state at higher P and ρ. P_1, ρ_1, and u_{p1} we determined from the measured shock velocity in the LiD immediately prior to reflection from the rear α-quartz window, along with a fit to the $U_s - u_p$ Principal Hugoniot data (listed in Table I). The measured shock velocity in the rear α-quartz window and the known Hugoniot of α-quartz provided the double-shocked P_2 and u_{p2} for LiD. The velocity

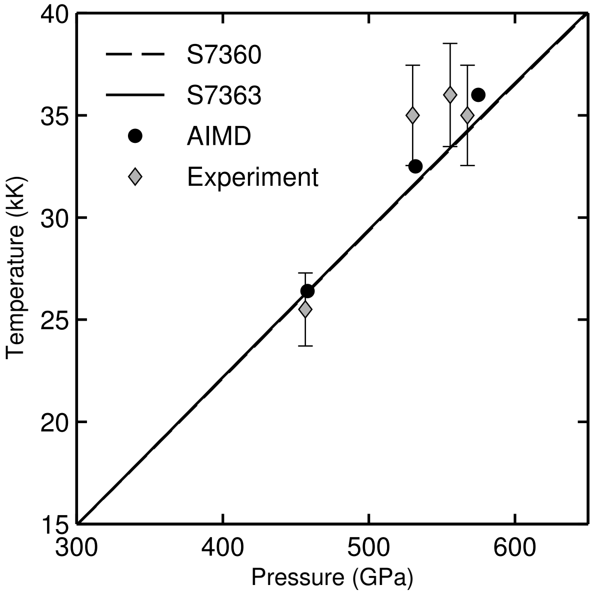

FIG. 9. LiD temperature along the Hugoniot. Solid (dashed) black line, SESAME 7363[15] (7360[10]); black cirlces, AIMD, this work. Gray diamonds, experiment, this work.

of the second shock in the LiD, U_{s2}^{LiD}, was then determined by evaluating Eq. (2) using the change in pressure and particle velocity, $(P_2 - P_1)$ and $(u_{p2} - u_{p1})$. Given U_{s2}^{LiD}, ρ_1, and $(u_{p2} - u_{p1})$, the reshock density, ρ_2, was determined from Eq. (3). Using the Monte Carlo technique, the one-sigma uncertainties in P_2 and ρ_2 for the reshock states were found to be ~0.5-1% and ~1-2%, respectively. Although the uncertainty for the reshock data is larger than that for the principal Hugoniot data (entirely due to the larger uncertainty in the initial state), the accuracy of the present data provide a stringent constraint of the reshock response of LiD in the multi-Mbar regime.

The pertinent parameters for these reshock experiments are listed in Table II. U_s^{LiD} and U_2^{Q} denote the measured shock velocities in the LiD sample and the rear α-quartz window, respectively. P_1 and ρ_1 denote the density and pressure of the LiD in the Hugoniot state immediately prior to the shock reflecting from the rear α-quartz window, respectively, and P_2 and ρ_2 denote the inferred P and ρ of the LiD in the reshocked state, respectively.

The reshock data for LiD are shown in Fig. 10, where first shock states are shown as diamonds; the light gray points correspond to the principal Hugoniot measurements listed in Table I, and plotted in Fig. 7, while the dark gray points correspond to the state immediately prior to reshock, as determined by U_{s1}^{LiD} immediately prior to reshock and a fit to the

TABLE II. LiD reshock data. U_{s1}^{LiD} (U_{s2}^{Q}) is the measured shock velocity in the LiD sample (rear α-quartz window) immediately prior to (after) reflection from the rear α-quartz window. P_1 and $\rho 1$ are the inferred pressure and density in the shocked LiD sample, as determined from U_{s1}^{LiD} and a fit to the Hugoniot data in Table I. P_2 and ρ_2 are the inferred pressure and density in the reshocked state, respectively.

Expt	U_{s1}^{LiD} (km/s)	U_{s2}^{Q} (km/s)	P_1 (GPa)	ρ_1 (g/cm^3)	P_2 (GPa)	ρ_2 (g/cm^3)
Z2497N	26.94 ± 0.06	21.33 ± 0.03	429.1 ± 2.6	2.644 ± 0.023	728.4 ± 3.9	3.464 ± 0.056
Z2497S	28.60 ± 0.06	22.66 ± 0.03	491.0 ± 2.8	2.744 ± 0.024	837.1 ± 4.3	3.589 ± 0.057
Z2577	29.65 ± 0.06	23.43 ± 0.03	532.0 ± 3.0	2.797 ± 0.025	904.0 ± 4.5	3.696 ± 0.060
Z2692	29.85 ± 0.06	23.56 ± 0.03	540.0 ± 3.0	2.806 ± 0.025	915.6 ± 4.6	3.730 ± 0.061

Hugoniot data in Table I. The reshock states are shown as dark gray triangles. Also shown are the Principal and reshock Hugoniots from SESAME 7360 (dashed black line) and 7363 (solid black line), along with individually calculated AIMD Hugoniot and reshock states (black circles). Note that the experimental reshock data appear to be systematically softer than the AIMD predictions, similar to the trend observed for the Principal Hugoniot. Since we did not have access to a $^{\mathrm{n}}$LiD version of either SESAME 7247 or X2040 we were unable to make reshock comparisons with these models.

V. REANALYSIS OF NUCLEAR DRIVEN EXPERIMENTS

Ragan[2,3] published results of nuclear driven experiments on both ^{6}LiD and ^{6}LiH. Both of these publications suggest a somewhat more compressible response than all of the models considered here, including X2040. However, two aspects of the experiments and analysis bring into question the reported results; (*i*) the treatment of the shock standards upon release, and (*ii*) the steadiness of the shock and how that was accounted for in the analysis. Both of these aspects of the experimental analysis tend to result in a softer response. Thus, reanalysis tends to result in a stiffer response, bringing the inferred results into better agreement with the recent calculations and experiments.

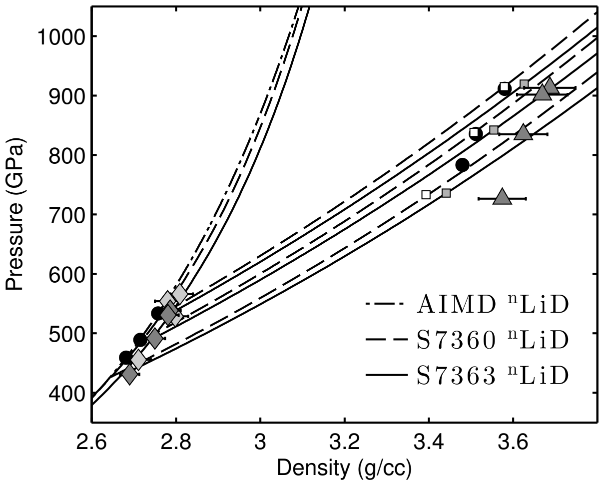

FIG. 10. LiD reshock data. Dashed (solid) black line, Principal and reshock Hugoniots for SESAME 7360[10] (7363[15]); dot-dashed black line, Principal and reshock Hugoniots for AIMD, this work. Light gray diamonds, Principal Hugoniot from IM measurements; Dark gray diamonds (triangles), inferred P and ρ immediately prior to (after) reshock; P_1 and ρ_1 were determined by U_{s1}^{LiD} and a fit to the Hugoniot data in Table I. White (gray) squares, reshock states from α-quartz rear window for SESAME 7360 (7363); black circles, reshock states for AIMD.

A. Shock Standards

Both molybdenum and beryllium were used as standards for the ^{6}LiD experiments reported in Ref. 2. According to Ref. 2, SESAME tables 2981 and 2020 were used for molybdenum and beryllium, respectively. Table 2981 was a new table developed by Kerley specifically for the analysis of this particular nuclear-driven experiment. Comparing the Hugoniot response of 2981 and the older 2980 to experimental data in the several TPa range from Ragan,[35] Al'tshuler et al.,[36] Trunin et al.,[37] and Mitchell et al.[38] (the Mitchell et al. results were reanalyzed with a more reasonable aluminum Hugoniot,[39] resulting in slightly higher inferred P and ρ) shows that 2981 is significantly stiffer than 2980, and is in better agreement with available data.

However, as Ragan points out, the release isentropes for 2981 and 2980 from the inferred shocked states of the molybdenum base plate (which differ in particle velocity by 3% for the two tables) are nearly identical in the vicinity of the ^{6}LiD Hugoniot. This is rather surprising. One would expect the release from these pressures and temperatures (5 TPa and 15 eV) to be adequately described by a Mie-Gruneisen (MG) model with Gamma (Γ)

of ∼2/3.[18,39] Comparing release isentropes from 2981 and 2980 with such a model suggests that 2981 is the outlier, inferring a release path that exhibits too high a particle velocity for a given pressure. To perform the reanalysis of this datum the 2981 Hugoniot was used as a reference for a MG model with Γ of 2/3.

For the beryllium standard experiment, Ragan used SESAME table 2020. Several different beryllium EOS tables were evaluated with respect to Hugoniot data in the few TPa range from Ragan[2] and Nellis et al.[40] (the Nellis et al. data was reanalyzed with a more reasonable aluminum Hugoniot, resulting in slightly higher inferred P and ρ). The most reasonable agreement with these data was found for table 2010,[41] which is a table developed by Kerley circa 2002. To perform a reanalysis of this datum, the SESAME 2010 Hugoniot was used as a reference for a MG model with Γ of 2/3.

The final experiment,[3] used carbon as the standard. Unfortunately, there is no Hugoniot data in the TPa range for comparison, and so SESAME table 7831 was used, the same table used by Ragan in his analysis. However, again the SESAME 7831 Hugoniot was used as the reference for a MG model with Γ of 2/3.

B. Attenuation Correction

Ragan noted that there was evidence of attenuation of the shock waves as they traversed the various layers (Mo/LiD/Be and Mo/Be/LiD for the ^{6}LiD experiments[3]). To account for this, it appears that Ragan assumed a 1% attenuation in shock velocity across the various samples. He then used the appropriate upshifted or downshifted velocity as the shock velocity at the front or rear of the material when performing the impedance match calculation. This correction results in a less compressible response than one would get if the average shock velocities obtained directly from the transit time measurements were used, ignoring the effects of attenuation. Furthermore, if one were to assume a larger attenuation (i.e. a larger percentage drop in shock velocity across the sample), the corrected result would be even less compressible.

It is interesting that the assumed attenuation for the ^{6}LiH experiment, 3%, is significantly larger than that assumed for the ^{6}LiD experiments, particularly given that the experimental configuration for the EOS package was nearly identical to that used in the ^{6}LiD study. Indeed the thicknesses of the lead, molybdenum, and the various samples were essentially the same

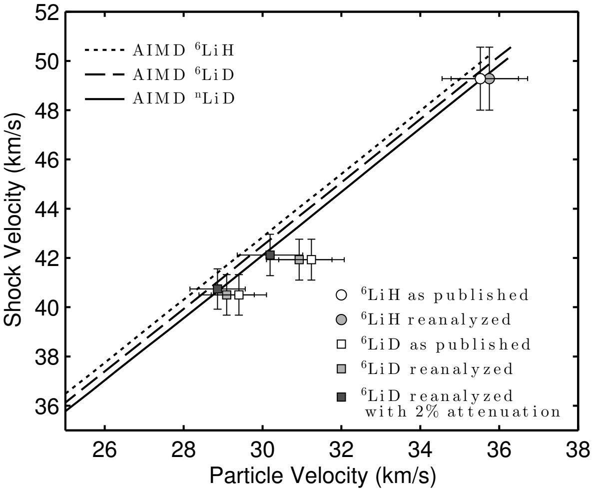

FIG. 11. Reanalysis of Ragan[2,3] results compared to AIMD Hugoniots. White (light gray) symbols, as published (reanalyzed) results. Dark gray symbols are reanalyzed results for ^{6}LiD assuming a 2% attenuation of the shock (as opposed to 1%).

for the two studies. The only difference being that the shocked state in the molybdenum was higher (∼6 TPa) for the ^{6}LiH experiment than it was (∼5 TPa) for the ^{6}LiD experiments. It is not clear why the attenuation was assumed to be larger, but it does question the magnitude of the attenuation used to correct the ^{6}LiD data. If one were to assume that the magnitude of the attenuation was underestimated in the ^{6}LiD experiments, the correction for attenuation would be larger and would bring the inferred results closer in line with the recent AIMD calculations for ^{6}LiD, as shown in Fig. 11. This figure shows the reanalyzed results along with the AIMD Hugoniots for ^{6}LiH, ^{6}LiD, and ^{n}LiD. Given this exercise, it can be concluded that the results from the nuclear driven experiments are consistent with the recent theoretical and experimental studies of LiD.

VI. CONCLUSSION

A series of shock compression experiments were performed on LiD single crystals using the high velocity flyer plate capability of the Sandia Z Machine. Pressure, density, and temperature were measured along the Principal Hugoniot between ∼190-570 GPa. Pressure and density of reshock states were also measured up to ∼920 GPa. These data were found to be in disagreement with the legacy equation of state (EOS) models at LLNL and LANL, X2040 and S7247, respectively. In contrast, the results were found to be in reasonably good agreement with recent *ab-initio* molecular dynamics calculations performed in this study, as well as two new EOS models, SESAME 7360 and 7363, developed at LANL.[10,15] Finally, legacy nuclear driven experiments[2,3] on ^{6}LiD and ^{6}LiH were reanalyzed, using modern EOS tables and better release models. The reanalyzed data were found to be consistent with the recent theoretical and experimental work on LiD.

ACKNOWLEDGMENTS

We would like to thank Dan Dolan for locating the single crystal LiD boule. Michael Siegal is thanked for providing access to the argon glove box used in target preparation. Mark Rodriguez and Jeff Reich are thanked for performing x-ray diffraction and inductively coupled plasma mass spectrometry measurements, respectively, to characterize the sample material used in these experiments. We also thank the large team at Sandia that contributed to the design and fabrication of the flyer plate loads and the fielding of the shock diagnostics. Sandia National Laboratories is a multi-mission laboratory managed and operated by Sandia Corporation, a wholly owned subsidiary of Lockheed Martin Corporation, for the U.S. Department of Energy's National Nuclear Security Administration under Contract No. DE-AC04-94AL85000.

REFERENCES

[1] S. P. Marsh, ed., *LASL Shock Hugoniot Data* (University of California Press, Berkeley CA, 1980).

[2] C. E. Ragan III, Phys. Rev. A **25**, 3360 (1982).

[3] C. E. Ragan III, Phys. Rev. A **29**, 1391 (1984).

[4] P. Loubeyre, R. L. Toullec, M. Hanfland, L. Ulivi, F. Datchi, and D. Hausermann, Phys. Rev. B **57**, 10403 (1998).

[5] A. L. Kritcher, P. Neumayer, C. R. D. Brown, P. Davis, T. Döppner, R. W. Falcone, D. O. Gericke, G. Gregori, B. Holst, O. L. Landen, H. J. Lee, E. C. Morse, A. Pelka, R. Redmer, M. Roth, J. Vorberger, K. Wünsch, and S. H. Glenzer, Phys. Rev. Lett. **103**, 245004 (2009).

[6] J. Hama, K. Suito, and N. Kawakami, Phys. Rev. B **39**, 3351 (1989).

[7] R. Ahuja, O. Eriksson, and B. Johanssen, Physica B: Cond Matter **265**, 87 (1999).

[8] T. Ogitsu, E. Schwegler, F. Gygi, and G. Galli, Phys. Rev. Lett. **91**, 175502 (2003).

[9] S. Lebègue, M. Alouani, B. Arnaud, and W. E. Pickett, Europhys. Lett. **63**, 562 (2003).

[10] D. Sheppard, J. D. Kress, S. Crockett, L. A. Collins, and M. P. Desjarlais, Phys. Rev. E **90**, 063314 (2014).

[11] D. A. Horner, J. D. Kress, and L. A. Collins, Phys. Rev. B **77**, 064102 (2008).

[12] D. A. Horner, F. Lambert, J. D. Kress, and L. A. Collins, Phys. Rev. B **80**, 024305 (2009).

[13] P. Stern, personal communication (2014).

[14] S. P. Lyon and J. D. Johnson, *SESAME: The Los Alamos National Laboratory Equation of State Database*, Technical Report No. LA-UR-92-3407 (Los Alamos National Laboratory, 1992).

[15] D. G. Sheppard, J. D. Kress, S. Crockett, L. A. Collins, and C. W. Greeff, *SESAME 7363: A New Li(6)D Equation of State*, Technical Report No. LA-UR-15-27354 (Los Alamos National Laboratory, 2015).

[16] M. Matzen *et al.*, Phys. Plasmas **12**, 055503 (2005).

[17] M. D. Knudson and M. P. Desjarlais, Phys. Rev. Lett **103**, 225501 (2009).

[18] M. D. Knudson and M. P. Desjarlais, Phys. Rev. B **88**, 184107 (2013).

[19] K. J. R. Rossman and P. D. P. Taylor, Pure Appl. Chem. **71**, 1593 (1999).

[20] J. L. Anderson, J. Nasise, K. Philipson, and F. E. Pretzel (deceased), J. Phys. Chem. Solids **31**, 613 (1970).

[21] E. Staritzky and D. I. Walker, Anal. Chem. **28**, 1055 (1956).

[22] R. Lemke, M. D. Knudson, A. Robinson, T. Haill, K. Struve, J. Asay, and T. Mehlhorn, Phys. Plasmas **10**, 1867 (2003).

[23] R. Lemke, M. D. Knudson, and J.-P. Davis, Int. J. Impact Eng. **38**, 480 (2011).

[24] L. M. Barker and R. E. Hollenbach, J. Appl. Phys. **43**, 4669 (1972).

[25] G. Ghosh, Opt. Commun. **163**, 95 (1999).

[26] R. M. Summers, J. S. Perry, M. W. Wong, E. S. Hertel, Jr., T. G. Trucano, and L. C. Chhabildas, Int. J. Impact Eng. **20**, 779 (1997).

[27] R. Lemke, M. D. Knudson, D. E. Bliss, K. Cochrane, J.-P. Davis, A. A. Giunta, H. C. Harjes, and S. A. Slutz, J. Appl. Phys. **98**, 073530 (2005).

[28] G. I. Kerley, Int. J. Impact Eng. **5**, 441 (1987).

[29] G. Kerley, *Equations of State for Composite Materials*, Kerley Publishing Services Report No. KPS99-4 (Kerley Publishing Services, 1999).

[30] G. E. Duvall and R. A. Graham, Rev. Mod. Phys. **49**, 523 (1977).

[31] M. D. Knudson, M. P. Desjarlais, R. W. Lemke, T. R. Mattsson, M. French, N. Nettelmann, and R. Redmer, Phys. Rev. Lett **108**, 091102 (2012).

[32] G. Kresse and J. Furthmüller, Phys. Rev. B **54**, 11169 (1996).

[33] G. Kresse and D. Joubert, Phys. Rev. B **59**, 1758 (1999).

[34] P. M. Celliers, P. Loubeyre, J. H. Eggert, S. Brygoo, R. S. McWilliams, D. G. Hicks, T. R. Boehly, R. Jeanloz, and G. W. Collins, Phys. Rev. Lett. **104**, 184503 (2010).

[35] C. E. Ragan III, M. G. Silbert, and B. C. Diven, J. Appl. Phys. **48**, 2860 (1977).

[36] L. V. Al'tshuler, A. A. Bakanova, I. P. Dudoladov, E. A. Dynin, R. F. Trunin, and B. S. Chekin, J. Appl. Mech. Tech. Phys. **22**, 145 (1981).

[37] R. F. Trunin, G. V. Simakov, Y. N. Sutulov, A. B. Medvedev, B. D. Rogozkin, and Y. E. Fedorov, Sov. Phys. - JETP **69**, 580 (1989).

[38] A. C. Mitchell, W. J. Nellis, J. A. Moriarty, R. A. Heinle, N. C. Holmes, R. E. Tipton, and G. W. Repp, J. Appl. Phys. **69**, 2981 (1991).

[39] M. D. Knudson, M. P. Desjarlais, and A. Pribram-Jones, Phys. Rev. B **91**, 224105 (2015).

[40] W. J. Nellis, J. A. Moriarty, A. C. Mitchell, and N. C. Holmes, J. Appl. Phys. **85**, 2225 (1997).

[41] G. Kerley, *Equations of State for Be, Ni, W, and Au*, SAND2003-3784 (Sandia Report, 2003).